UCRL-JRNL-209252

LAWRENCE
LIVERMORE
NATIONAL
LABORATORY

Estimates and Rigorous Bounds on Pore-Fluid Enhanced Shear Modulus in Poroelastic Media with Hard and Soft Anisotropy

J. G. Berryman

January 27, 2005

International Journal of Damage Mechanics

Disclaimer

Submitted to : *International Journal of Damage Mechanics*

Estimates and Rigorous Bounds on Pore-Fluid Enhanced Shear Modulus in Poroelastic Media with Hard and Soft Anisotropy

James G. Berryman[1,*]

[1] *University of California, Lawrence Livermore National Laboratory, P.O.Box 808 L-200, Livermore, CA 94551-9900, USA*

(Dated: January 24, 2005)

* berryman1@llnl.gov

Abstract

A general analysis of poroelasticity for hexagonal, tetragonal, and cubic symmetry shows that four eigenvectors are pure shear modes with no coupling to the pore-fluid mechanics. The remaining two eigenvectors are linear combinations of pure compression and uniaxial shear, both of which are coupled to the fluid mechanics. The analysis proceeds by first reducing the problem to a 2×2 system. The poroelastic system including both anisotropy in the solid elastic frame (*i.e.*, with "hard anisotropy"), and also anisotropy of the poroelastic coefficients ("soft anisotropy") is then studied in some detail. In the presence of anisotropy and spatial heterogeneity, mechanics of the pore fluid produces shear dependence on fluid bulk modulus in the overall poroelastic system. This effect is always present (though sometimes small in magnitude) in the systems studied, and can be comparatively large (up to a maximum increase of about 20 per cent) in some porous media — including porous glass and Schuler-Cotton Valley sandstone. General conclusions about poroelastic shear behavior are also related to some recently derived product formulas that determine overall shear response of these systems. Another method is also introduced based on rigorous Hashin-Shtrikman-style bounds for nonporous random polycrystals, followed by related self-consistent estimates of mineral constants for polycrystals. Then, another self-consistent estimation method is formulated for the porous case, and used to estimate drained and undrained effective constants. These estimates are compared and contrasted with the results of the first method and a consistent picture of the overall behavior is found in three computed examples for polycrystals of grains having tetragonal symmetry.

INTRODUCTION

Although evidence of pore-fluid enhancement of shear modulus in anisotropic poroelastic media has been known for some time, little analysis of this phenomenon has been available in the literature. For example, an important paper by Gassmann (1951) concerns the effects of fluids on the mechanical properties of porous rock. His main result is the well-known fluid-substitution formula (that now bears his name) for the bulk modulus in undrained, isotropic poroelastic media. He also postulated that the effective shear modulus would be independent of the mechanical properties of the fluid when the medium is isotropic. That the independence of shear modulus from fluid effects is guaranteed for isotropic media at very low or quasistatic frequencies was shown recently by Berryman (1999) to be tightly coupled to the original bulk modulus result of Gassmann; each result implies the other in isotropic media. It has gone mostly without discussion in the literature that Gassmann (1951) also derived general results for anisotropic porous rocks in the same 1951 paper. It is not hard to see that these results imply, contrary to the isotropic case, that the overall undrained shear modulus in fact generally does depend on fluid properties in anisotropic media. However, Gassmann's paper does not remark at all on this difference in behavior between isotropic and anisotropic porous rocks. Brown and Korringa (1975) also address the same class of problems, including both isotropic and anisotropic cases, but again they do not remark on the shear modulus results in either case.

On the other hand, Hudson (1981), in his early work on cracked solids, explicitly demonstrates differences between fluid-saturated and dry cracks and relates his work to that of Walsh (1969) and O'Connell and Budiansky (1974), but does not make any connection to the work of either Gassmann (1951), or Brown and Korringa (1975). Mukerji and Mavko (1994) show numerical results based on work of Gassmann (1951), Brown and Korringa (1975) and Hudson (1981) demonstrating the fluid dependence of shear in anisotropic rock, but again they do not remark on these results at all. Mavko and Jizba (1991) use a simple reciprocity argument to establish a direct, but approximate, connection between undrained shear response and undrained compressional response in rocks containing cracks. Berryman and Wang (2001) show that deviations from Gassmann's results sufficient to produce shear modulus dependence on fluid mechanical properties require the presence of anisotropy on the microscale, thereby explicitly violating the microhomogeneous and microisotropy conditions implicit in Gassmann's original derivation. Berryman *et al.* (2002a) go further and make use of differential effective medium analysis to show explicitly how the undrained, overall isotropic shear modulus can depend on fluid trapped in penny-shaped cracks. Meanwhile, laboratory results [see Berryman *et al.* (2002b)] show conclusively that the shear modulus does depend on fluid mechanical properties for low-porosity, low-permeability rocks, and high-frequency laboratory experiments ($f > 500$ kHz).

A simple example showing how the presence of anisotropy influences the shear modulus, and specifically how the shear modulus becomes fluid dependent would be most helpful for our intuition in poromechanics. The purpose of this work is therefore to demonstrate in some detail how the shear behavior becomes dependent on fluid properties in anisotropic media. Two distinct but related analyses addressing this topic have been presented recently by the author (Berryman, 2004a; 2005). Both of these papers made explicit use of layered media — having layers composed of isotropic poroelastic materials — together with exact results for such media based on Backus averaging (Backus, 1962). In contrast, the present analysis does *not* make use of such a specific model. To separate the part of the system response due to poroelastic effects, from the part that would be present in any elastic material, we specifically distinguish two possible sources of anisotropy: the elastic, or "hard," anisotropy, and the poroelastic, or "soft," anisotropy arising from pore-pressure effects. Both types of anisotropy will be present in the study that follows.

Our analysis for hexagonal, tetragonal, and cubic media is presented in the next three sections. In particular the "Eigenvectors" section also introduces the effective undrained shear modulus relevant to our general discussion. Examples are presented for glass and one sandstone. The paper's results and conclusions are summarized in the final section. Two Appendices collect some mathematical details needed in the main text. In particular, Appendix B provides a different and more general proof of the product formulas used repeatedly in the text.

FLUID-SATURATED POROELASTIC MEDIA

In contrast to traditional elastic analysis, the presence in rock of a saturating pore fluid introduces an additional control field and an additional type of strain variable. The pressure p_f in the fluid is a new field parameter that can be controlled. Allowing sufficient time for global pressure equilibration will permit us to consider p_f to be a constant throughout the percolating (connected) pore fluid, while restricting the analysis to quasistatic processes. The change ζ in the amount of fluid mass contained in the pores [see Biot (1962) or Berryman and Thigpen (1985)] is a new type of strain variable, measuring how much of the original fluid in the pores is squeezed out during the compression of the pore volume while including the effects of compression or expansion of the pore fluid itself due to changes in p_f. It is most convenient to write the resulting equations in terms of compliances rather than stiffnesses, so the basic equation to be considered takes the following form for isotropic media:

$$\begin{pmatrix} e_{11} \\ e_{22} \\ e_{33} \\ -\zeta \end{pmatrix} = \begin{pmatrix} s_{11} & s_{12} & s_{12} & -\beta \\ s_{12} & s_{11} & s_{12} & -\beta \\ s_{12} & s_{12} & s_{11} & -\beta \\ -\beta & -\beta & -\beta & \gamma \end{pmatrix} \begin{pmatrix} \sigma_{11} \\ \sigma_{22} \\ \sigma_{33} \\ -p_f \end{pmatrix}, \tag{1}$$

where e_{ij} and σ_{ij} for $i,j = 1,2,3$ are the components of overall strain and stress, respectively, in 3D. The constants appearing in the matrix on the right hand side will be defined in the following two paragraphs. The compliances s_{ij} appearing in (1) are simply related to the drained elastic constants λ_d and G_d in the same way they are related in normal elasticity. So, we find that

$$s_{11} = \frac{1}{E_d} = \frac{\lambda_d + G_d}{G_d(3\lambda_d + 2G_d)} \tag{2}$$

and

$$s_{12} = -\frac{\nu_d}{E_d}, \tag{3}$$

where the drained Young's modulus E_d is defined by the second equality of (2) and the drained Poisson's ratio is determined by

$$\nu_d = \frac{\lambda_d}{2(\lambda_d + G_d)}. \tag{4}$$

When the external stress is hydrostatic so $\sigma = \sigma_{11} = \sigma_{22} = \sigma_{33}$, equation (1) telescopes down to

$$\begin{pmatrix} e \\ -\zeta \end{pmatrix} = \frac{1}{K_R^d} \begin{pmatrix} 1 & -\alpha \\ -\alpha & \alpha/B \end{pmatrix} \begin{pmatrix} \sigma \\ -p_f \end{pmatrix}, \tag{5}$$

where $e = e_{11} + e_{22} + e_{33}$, $K_R^d = \lambda_d + \frac{2}{3}G_d$ is the drained bulk modulus, $\alpha = 1 - K_R^d/K_m$ is the Biot-Willis parameter (Biot and Willis, 1957) with K_m being the bulk modulus of the solid minerals present, and Skempton's pore-pressure buildup parameter B (Skempton, 1954) is given by

$$B = \frac{1}{1 + K_p(1/K_f - 1/K_m)}. \tag{6}$$

New parameters appearing in (6) are the bulk modulus of the pore fluid K_f and the pore modulus $K_p^{-1} = \alpha/\phi K_R^d$ where ϕ is the porosity. The expressions for α and B can be generalized slightly by supposing that the solid frame is composed of more than one constituent, in which case the K_m appearing in the definition of α is replaced by K_s and the K_m appearing explicitly in (6) is replaced by K_ϕ [see Brown and Korringa (1975), Rice and Cleary (1976), Berryman and Milton (1991), Berryman and Wang (1995)]. This is an important additional complication (Berge and Berryman, 1995). We choose not to pursue this issue further here.

Comparing (1) and (5), we find for an isotropic system that

$$\beta = \frac{\alpha}{3K_R^d} \tag{7}$$

and

$$\gamma = \frac{\alpha}{BK_R^d}. \tag{8}$$

RELATIONS FOR ANISOTROPY IN POROELASTIC MATERIALS

Gassmann (1951), Brown and Korringa (1975), and many others have considered the problem of obtaining effective constants for anisotropic poroelastic materials when the pore fluid is confined within the pores. The confinement condition amounts to a constraint that the increment of fluid content $\zeta = 0$, while the external loading σ is changed and the pore-fluid pressure p_f is allowed to equilibrate.

To recall an elementary derivation of the Gassmann equation for anisotropic materials, we consider the anisotropic generalization of (1), which is

$$\begin{pmatrix} e_{11} \\ e_{22} \\ e_{33} \\ -\zeta \end{pmatrix} = \begin{pmatrix} s_{11} & s_{12} & s_{13} & -\beta_1 \\ s_{12} & s_{22} & s_{23} & -\beta_2 \\ s_{13} & s_{23} & s_{33} & -\beta_3 \\ -\beta_1 & -\beta_2 & -\beta_3 & \gamma \end{pmatrix} \begin{pmatrix} \sigma_{11} \\ \sigma_{22} \\ \sigma_{33} \\ -p_f \end{pmatrix}. \tag{9}$$

The three simple (uncoupled) shear contributions for hexagonal, tetragonal, orthorhombic, and/or cubic symmetries have been immediately excluded from consideration, since they can easily be seen not to interact mechanically with the fluid effects. Since this form includes only orthorhombic, tetragonal, cubic, hexagonal, and all isotropic systems, it is not completely general. But our goal is an analytical level of understanding, rather than great generality. We are also assuming that the material axes are aligned with the spatial axes. This latter assumption is not significant however for the derivation that follows. Such an assumption is important when properties of laminated materials having arbitrary orientation relative to the spatial axes need to be considered, but this issue is not studied here.

If the fluid is confined (or undrained on the time scales of interest to applications in high frequency wave propagation), then $\zeta \equiv 0$ in (9) and p_f becomes a linear function of σ_{11}, σ_{22}, σ_{33}. Eliminating p_f from the resulting equations, we obtain the general expression for the strain dependence on external stress under such undrained conditions:

$$\begin{pmatrix} e_{11} \\ e_{22} \\ e_{33} \end{pmatrix} = \left[\begin{pmatrix} s_{11} & s_{12} & s_{13} \\ s_{12} & s_{22} & s_{23} \\ s_{13} & s_{23} & s_{33} \end{pmatrix} - \gamma^{-1} \begin{pmatrix} \beta_1 \\ \beta_2 \\ \beta_3 \end{pmatrix} \begin{pmatrix} \beta_1 & \beta_2 & \beta_3 \end{pmatrix} \right] \begin{pmatrix} \sigma_{11} \\ \sigma_{22} \\ \sigma_{33} \end{pmatrix}$$

$$\equiv \begin{pmatrix} s^u_{11} & s^u_{12} & s^u_{13} \\ s^u_{12} & s^u_{22} & s^u_{23} \\ s^u_{13} & s^u_{23} & s^u_{33} \end{pmatrix} \begin{pmatrix} \sigma_{11} \\ \sigma_{22} \\ \sigma_{33} \end{pmatrix}. \tag{10}$$

The compliances s_{ij}'s are the fluid-drained constants, while the compliances s^u_{ij}'s are the fluid-undrained (or fluid-confined) constants.

The fundamental result (10) was obtained earlier by both Gassmann (1951) and Brown and Korringa (1975), and may be written simply as

$$s^u_{ij} = s_{ij} - \frac{\beta_i \beta_j}{\gamma}, \quad \text{for} \quad i, j = 1, 2, 3. \tag{11}$$

Eq. (11) is the anisotropic generalization of the well-known Gassmann equation for isotropic, microhomogeneous porous media.

EIGENVECTORS FOR HEXAGONAL, TETRAGONAL, AND CUBIC SYMMETRY

The 3×3 system (10) can be analyzed most easily in terms of its eigenfunctions and eigenvalues. However, such very general results do not necessarily provide the kind of insight into the poromechanics we are trying to gain. So instead of proceeding in this direction, we will now restrict attention to three common types of anisotropy: hexagonal (transverse isotropy), tetragonal, and cubic symmetry. Transverse isotropy is relevant in particular to many layered earth materials and also industrial systems. But all three types of symmetry are useful to us here because we can immediately eliminate one of the eigenvectors from consideration. Furthermore, the three remaining shear modes (equations not shown here) are uncoupled – both from each other and from the part of the poroelastic tensor we will study in most detail. [We could also study trigonal symmetry using a very analogous methods, but instead choose to avoid this here as trigonal systems have two types of coupling that tend to complicate the analysis somewhat.]

The three types of crystal symmetry considered here are:

(a) Hexagonal symmetry: requiring $s_{11} = s_{22}$, $s_{13} = s_{23}$, $s_{44} = s_{55}$, and s_{66} is coupled to s_{11} and s_{12}.

(b) Tetragonal symmetry [classes $4mm$, $\bar{4}2m$, $4/mmm$ – see Nye (1957) for details]: requiring $s_{11} = s_{22}$, $s_{13} = s_{23}$, $s_{44} = s_{55}$, and (unlike hexagonal symmetry) s_{66} is not coupled to s_{11} and s_{12}.

(c) Cubic symmetry (actually a special case of tetragonal symmetry): requiring $s_{11} = s_{22} = s_{33}$, $s_{12} = s_{13} = s_{23}$, and $s_{44} = s_{55} = s_{66}$. Again, s_{66} is not coupled to s_{11} and s_{12}.

For all of these crystal symmetries, we assume that the poroelastic coupling coefficients satisfy $\beta_1 = \beta_2$, and β_3 can be independent of the other two coefficients.

Three mutually orthogonal (but unnormalized) vectors of interest are:

$$v_1 = \begin{pmatrix} 1 \\ 1 \\ 1 \end{pmatrix}, \qquad v_2 = \begin{pmatrix} 1 \\ -1 \\ 0 \end{pmatrix}, \qquad v_3 = \begin{pmatrix} 1 \\ 1 \\ -2 \end{pmatrix}. \tag{12}$$

Treating these vectors as stresses, the first corresponds to a simple hydrostatic stress, the second to a planar shear stress, and the third to a uniaxial shear stress (*i.e.*, the shear component of a pure uniaxial principal stress applied along the z-axis — which is also the same as the symmetry axis for a layered system). Thus, it is apparent that — for the crystal symmetries considered — the planar shear stress v_2 is an eigenvector of the system, and, furthermore, it results in no contribution from the pore fluid. Therefore, this vector will be of no interest here, and the system for all three crystal symmetries can then be reduced to 2×2.

Because the tetragonal symmetry considered here has the hexagonal and cubic symmetries as special cases, we will phrase the following discussion in terms of tetragonal symmetry until we need to discuss detailed results at the end of the calculation.

Compliance Formulation

If we define the effective compliance matrix for the system as S^* having the matrix elements given in (11), then the bulk modulus for this system is defined in terms of v_1 by

$$\frac{1}{K_R^u} = v_1^T S^u v_1 = \frac{1}{K_R^d} - \gamma^{-1}\left(2\beta_1 + \beta_3\right)^2 = \frac{1 - \alpha B}{K_R^d}, \tag{13}$$

where the T superscript indicates the transpose, and $1/K_R^d \equiv \sum_{i,j=1}^{3} s_{ij}$. The result (13) is usually quoted as Gassmann's equation for the bulk modulus of an undrained (or confined fluid) anisotropic porous system. Also, note that in general

$$\frac{1}{\gamma}\sum_{i=1}^{3}\beta_i = \frac{2\beta_1 + \beta_3}{\gamma} = B, \tag{14}$$

where $2\beta_1 + \beta_3 = \alpha/K_R^d$. The vector v_1 is not an eigenvector of this system, but nevertheless plays a fundamental role in the poromechanics.

The true eigenvectors of the subproblem of interest (*i.e.*, in the space orthogonal to the four pure shear eigenvectors already discussed and eliminated) are necessarily linear combinations of v_1 and v_3. We can construct the relevant contracted operator for the 2×2 subsystem by considering:

$$\begin{pmatrix} v_1^T \\ v_3^T \end{pmatrix} S^u \begin{pmatrix} v_1 & v_3 \end{pmatrix} \equiv \begin{pmatrix} 9A_{11}^u & 18A_{13}^u \\ 18A_{13}^u & 36A_{33}^u \end{pmatrix} \tag{15}$$

(in all cases u superscripts and subscripts indicate that the undrained pore-fluid effects are included) and the reduced matrix

$$\Sigma^u = A_{11}^u v_1 v_1^T + A_{13}^u (v_1 v_3^T + v_3 v_1^T) + A_{33}^u v_3 v_3^T, \tag{16}$$

where

$$\begin{aligned} A_{11}^u &= [2(s_{11}^u + s_{12}^u + 2s_{13}^u) + s_{33}^u]/9 = \frac{1}{9K_R^u}, \\ A_{13}^u &= (s_{11}^u + s_{12}^u - s_{13}^u - s_{33}^u)/9, \\ A_{33}^u &= (s_{11}^u + s_{12}^u - 4s_{13}^u + 2s_{33}^u)/18 = \frac{1}{12G_u^r}. \end{aligned} \tag{17}$$

We now proceed to interpret these constants in terms of their contributions to the shear modulus dependence on fluid content.

First we remark that

$$3A^u_{11} = \frac{1}{3K^u_R}, \tag{18}$$

where K^u_R is the undrained (or Gassmann) bulk modulus for the system in (13). Therefore, A^u_{11} is proportional to the undrained bulk compliance of this system. The other two distinct matrix elements cannot be given quite such simple interpretations. However, for the drained moduli, we have a general rule [see Appendix B and also Berryman (2004a)] stating that

$$6K^d_R G^v_d = 6K^d_V G^r_d = \left[\Lambda^d_+ \Lambda^d_-\right]^{-1}, \tag{19}$$

where the drained eigenvalues are

$$\Lambda^d_\pm = 3\left[A^d_{33} + A^d_{11}/2 \pm \sqrt{(A^d_{33} - A^d_{11}/2)^2 + 2(A^d_{13})^2}\right]. \tag{20}$$

The drained Voigt bulk modulus is determined by

$$K^d_V = [2(c_{11} + c_{12} + 2c_{13}) + c_{33}]/9 = A^d_{11}. \tag{21}$$

The drained Voigt uniaxial shear modulus is determined by

$$G^v_d = [c_{11} + c_{12} - 4c_{13} + 2c_{33}]/6, \tag{22}$$

and the drained Reuss uniaxial shear modulus is given similarly by

$$\frac{1}{2G^r_d} = [s_{11} + s_{12} - 4s_{13} + 2s_{33}]/3 = 3A^d_{33}, \tag{23}$$

Exactly analogous expressions hold for all the undrained coefficients, so we also have

$$6K^u_R G^v_u = 6K^u_V G^r_u = \left[\Lambda^u_+ \Lambda^u_-\right]^{-1}, \tag{24}$$

and all the definitions in (20)-(23) are then replaced by those with undrained quantities on the right hand side.

The eigenvectors $f(\theta)$ for the undrained problem (*i.e.*, for the reduced operator Σ^* for the pertinent $s \times 2$ system) necessarily take the form

$$f(\theta) = \frac{\cos\theta}{\sqrt{3}} v_1 + \frac{\sin\theta}{\sqrt{6}} v_3, \tag{25}$$

with two solutions for the rotation angle: θ_- and $\theta_+ = \theta_- + \frac{\pi}{2}$, guaranteeing that the two solutions (the eigenvectors) are orthogonal. It is easily seen that the eigenvalues are given by

$$\Lambda^u_\pm = 3\left[A^u_{33} + A^u_{11}/2 \pm \sqrt{(A^u_{33} - A^u_{11}/2)^2 + 2(A^u_{13})^2}\right] \tag{26}$$

so that

$$\Lambda^u_+\Lambda^u_- = 18\left[A^u_{11}A^u_{33} - (A^u_{13})^2\right]. \tag{27}$$

The rotation angles are determined by

$$\tan\theta^u_\pm = \frac{\Lambda^u_\pm/3 - A^u_{11}}{\sqrt{2}A^u_{13}} = \\ \left[A^u_{33} - A^u_{11}/2 \pm \sqrt{(A^u_{33} - A^u_{11}/2)^2 + 2(A^u_{13})^2}\right]/\sqrt{2}A^u_{13}. \tag{28}$$

One part of the rotation angle is due to the drained (fluid free) "hard anisotropic" nature of the rock frame material. We will call this part θ^d. The remainder is due to the presence of the fluid in the pores, and we will call this part $\delta\theta \equiv \theta^u - \theta^d$ for the "soft anisotropy." Using a standard formula for tangents, we have

$$\delta\theta_\pm = \tan^{-1}\left[\frac{\tan\theta^u_\pm - \tan\theta^d_\pm}{1 + \tan\theta^u_\pm \tan\theta^d_\pm}\right]. \tag{29}$$

Furthermore, formulas for $\theta^d_\pm$ are readily found from (28) by taking the poroelastic parameter $\gamma \to \infty$ (corresponding to air saturation of the pores).

Since

$$\tan\theta^u_+ \cdot \tan\theta^u_- = -1, \tag{30}$$

it is sufficient to consider just one of the signs in front of the radical in (28). The most convenient choice for analytical purposes turns out to be the minus sign (which corresponds to the eigenvector with the larger component of pure compression). Furthermore, it is also clear from the form of (28) that often the behavior of most interest to us here occurs for cases when $A^u_{13} \neq 0$ (since otherwise v_1 and v_3 are both eigenvectors and the shear modulus is uncoupled to the fluid effects).

To simplify the analysis we note that, at least for purposes of modeling, anisotropy of the compliances s_{ij} and the poroelastic coefficients β_i can be treated independently. We assume that anisotropy displayed in the s_{ij}'s corresponds mostly to the anisotropy in the solid elastic components of the system, while anisotropy in the β_i's corresponds mostly to anisotropy in the shapes and spatial distribution of the porosity. Thus, contributions to the anisotropy in the s_{ij}'s is the "hard anisotropy," and constributions to the anisotropy in the β_i's is the "soft anisotropy." Both types of anisotropy are considered in the following analysis.

In the limit of a nearly isotropic solid frame (so the "hard anisotropy" vanishes and thus we will also call this the "quasi-isotropic" limit), it is not hard to see that

$$A_{33}^u = \frac{1}{12G_u^r} = \frac{1}{12G_d^r} - \frac{(\beta_1 - \beta_3)^2}{9\gamma}, \tag{31}$$

where G_d^r is the drained (Reuss) uniaxial shear modulus of the anisotropic solid frame. Similarly, the remaining coefficient

$$A_{13}^u = \frac{(s_{11} + s_{12} - s_{13} - s_{33})}{9} - \frac{(\beta_1 - \beta_3)B}{9}, \tag{32}$$

where we used (14) to simplify the expression. In the isotropic limit, all the solid contributions would cancel in this formula.

Expanding the square root in (26), we also have

$$\Lambda_+^u = 6A_{33}^u + \Delta \quad \text{and} \quad \Lambda_-^u = 3A_{11}^u - \Delta, \tag{33}$$

where Δ is defined consistently by either of the two preceeding expressions or by $2\Delta \equiv \Lambda_+^u - \Lambda_-^u + 3A_{11} - 6A_{33}$.

Stiffness Formulation

The dual to the problem just studied replaces compliances everywhere with stiffnesses, and then proceeds as before. Equations (15)–(18) are replaced by

$$\begin{pmatrix} v_1^T \\ v_3^T \end{pmatrix} C^u \begin{pmatrix} v_1 & v_3 \end{pmatrix} \equiv \begin{pmatrix} 9D_{11}^u & 18D_{13}^u \\ 18D_{13}^u & 36D_{33}^u \end{pmatrix} \tag{34}$$

(in all cases the u superscripts and subscripts indicate that the pore-fluid effects are included) and the reduced matrix

$$(\Sigma^u)^{-1} = D_{11}^u v_1 v_1^T + D_{13}^u (v_1 v_3^T + v_3 v_1^T) + D_{33}^u v_3 v_3^T, \tag{35}$$

where

$$
\begin{aligned}
D_{11}^u &= [2(c_{11}^u + c_{12}^u + 2c_{13}^u) + c_{33}^u]/9 = K_V^u, \\
D_{13}^u &= (c_{11}^u + c_{12}^u - c_{13}^u - c_{33}^u)/9, \\
D_{33}^u &= (c_{11}^u + c_{12}^u - 4c_{13}^u + 2c_{33}^u)/18 = G_u^v/3.
\end{aligned}
\tag{36}
$$

It is a straightforward exercise to check that the two reduced problems are in fact inverses of each other. We will not repeat this analysis here. The main difference in the details is that the expressions for the D's in terms of the β's are rather more complicated than those for the compliance version, which is also why we choose to concentrate on the compliance formulation instead.

To illustrate the complications that arise, consider the bulk modulus upper bound K_V^u, which can be written in terms of compliances as

$$
\frac{1}{1/9K_V^u - s_{13}^u} = \frac{2}{s_{11}^u + s_{12}^u - 2s_{13}^u} + \frac{1}{s_{33}^u - s_{13}^u}, \tag{37}
$$

and which in turn can be rearranged into the form

$$
9K_V^u = \frac{s_{11}^u + s_{12}^u - 4s_{13}^u + 2s_{33}^u}{(s_{11}^u + s_{12}^u)s_{33}^u - 2(s_{13}^u)^2} = \frac{3/G_u^r}{2\Lambda_+^u\Lambda_-^u} \tag{38}
$$

Eq. (38) is perhaps the simplest expression possible for K_V^u in general. Even so, it is clearly much more complicated than (13) for K_R^u, and especially so when (11) is used to substitute for the s_{ij}^u values.

ESTIMATES OF UNDRAINED AND EFFECTIVE OVERALL SHEAR MODULI

Four shear moduli are easily defined for the anisotropic system under study. Furthermore, $G_2 = (c_{11} - c_{12})/2$, $G_3 = c_{44}$, $G_4 = c_{55}$, and $G_5 = c_{66}$. These moduli are all related to the four shear eigenvectors of the systems, and these do not couple to the pore-fluid mechanics. But, the eigenvectors in the reduced 2×2 system studied here are usually mixed in character, being quasi-compressional or quasi-shear modes. It is therefore somewhat problematic to find a proper definition for the fifth shear modulus. The author has analyzed this problem previously (Berryman, 2004b), and concluded that a sensible (though approximate) definition can be made using $G_1 = G_u^v$. There are several different ways of arriving at the same result, but for the present analysis the most useful of these is to express G_u^v in terms of the product $\Lambda_+^u\Lambda_-^u$ (the eigenvalue product, which is also the determinant of the 2×2 compliance system). The result [see Berryman (2004a) and a new derivation provided here in Appendix B for more details] is

$$\frac{1}{3K_R^u} \cdot \frac{1}{2G_u^v} \equiv \Lambda_+^u\Lambda_-^u = 18\left[A_{11}^u A_{33}^u - (A_{13}^u)^2\right]. \tag{39}$$

And, since $A_{11}^u = 1/9K_R^u$, we have

$$12\left[A_{33}^u - (A_{13}^u)^2/A_{11}^u\right] = \frac{1}{G_u^v} = \frac{1}{G_u^r} - \frac{4}{3}K_R^u\left(s_{11}^u + s_{12}^u - s_{13}^u - s_{33}^u\right)^2. \tag{40}$$

To obtain one estimate for an isotropic average overall undrained shear modulus, we next take the arithmetic mean of the five shear compliances. Prior work (Berryman, 2004a) has shown that the best choice of the undrained uniaxial shear compliance is $G_1^u = G_u^v$, while we have no flexibility for the other four values, being determined as they are by the eigenvalues. So we have:

$$\frac{1}{G_u^*} \equiv \frac{1}{5}\sum_{i=1}^{5}\frac{1}{G_i^u}, \tag{41}$$

and a similar expression for the drained estimate G_d^*.

Next, define

$$\tau_d \equiv s_{11} + s_{12} - s_{13} - s_{33}, \tag{42}$$

as well as the corresponding undrained quantity. Both of the these quantities will be needed in the formulas that follow. Combining these definitions and results for the difference between overall drained and undrained shear compliance gives:

$$\frac{1}{G_d^*} - \frac{1}{G_u^*} = \frac{1}{5}\left(\frac{1}{G_1^d} - \frac{1}{G_1^u}\right) = \frac{1}{5}\left(\frac{1}{G_d^v} - \frac{1}{G_u^v}\right) = \frac{4}{15}\frac{(K_R^d\tau_d + \beta_3' - \beta_1')^2}{1 - \alpha B}\frac{\alpha B}{K_R^d} = \frac{4}{15}\frac{(K_R^d\tau_d + \beta_3' - \beta_1')^2}{1 - \alpha B}\left[\frac{1}{K_R^d} - \frac{1}{K_R^u}\right]. \tag{43}$$

The β's appearing here are defined by $\beta_i' = \beta_i K_R^d/\alpha$. The final equality is presented to emphasize the similarity of the present results to those of Mavko and Jizba (1991) and Berryman *et al.* (2002b). In fact, by setting $\beta_1' = 0$, $\beta_3' = 1$ (maximal anisotropy), $B = 1$ (liquid saturation), $\tau_d = 0$ (hard isotropy), and $\alpha \simeq 0$ (very low porosity cracks) recovers the expressions of Mavko and Jizba (1991) for the case of a very dilute system of flat cracks in an isotropic background medium:

$$\frac{1}{G_d^*} - \frac{1}{G_u^*} = \frac{4}{15}\left[\frac{1}{K_R^d} - \frac{1}{K_R^u}\right]. \tag{44}$$

Note that (41) is just the Reuss average (lower bound) of the shear modulus. Also note that the definition (40) of G_u^v is actually based on the Voigt average. In terms of mathematical rigor, the result (43) therefore cannot be considered rigorous; it is neither an upper nor a lower bound. The justification for the formula comes not from absolute rigor, but instead from the observation (Berryman, 2004a) that G_u^v is in fact a very close estimate of the energy per unit volume in the fifth shear mode and from the knowledge that the Reuss average for compressional modulus tends to be much closer to observed results than the Voigt average does for many composite systems. So, for these reasons, the result (43) should be viewed, not as a rigorous formula (it is not), but it is nevertheless a good estimate of the undrained shear modulus.

The following section will present two examples of the use of these ideas for sample materials. After a brief discussion of these results, we will then present a more rigorous (but perhaps less insightful) approach and compare those results again to the ones presented in this section.

TABLE 1. Elastic and poroelastic parameters of the sandstone sample considered in the text. Bulk and shear moduli of the grains K_m and G_m, bulk and shear moduli of the drained porous frame K_R^d and G_d, the uniaxial and overall undrained shear moduli G_u^v and G_u^*, and the Biot-Willis parameter $\alpha = 1 - K_R^d/K_m$. The porosity is ϕ.

Elastic and Poroelastic Parameters	Schuler-Cotton Valley Sandstone
G_m (GPa)	36.7
G_u^* (GPa)	17.7
G_d (GPa)	15.7
G_u^v (GPa)	35.8
K_m (GPa)	41.8
K_R^d (GPa)	13.1
α	0.687
ϕ	0.033

SOME EXAMPLES AND DISCUSSION OF ESTIMATES

It is clear from (33) that fluid effects in Δ cannot increase the overall compliance eigenvalues simultaneously for both the quasi-bulk and the quasi-shear modes. Rather, if one increases, then the other must decrease. Furthermore, it is certainly always true that the presence of pore liquid either has no effect or else strengthens (*i.e.*, stiffens) the porous medium in compression. But this effect on the bulk modulus has been at least partially accounted for in $A^u_{11} = 1/9K^u_R$ through the original contribution derived by Gassmann (1951). The contribution of Δ to compliance cannot be so large as to offset the liquid effects on the undrained bulk modulus.

Examples of estimates

To clarify the situation, we show some examples in Figures 1–4. The details of the analysis that produces these figures are summarized in Appendix A. The main point is that, for the compliance version of the analysis, the contours of constant energy are ellipses when the vector f in (25) is interpreted as a stress. Analogously, when the vector is treated as a strain, the contours of constant energy are ellipses for the dual (or stiffness) formulation. If we choose to think of these figures as diagrams in the complex plane, then we note that — while circles and lines transform to circles and lines when transforming back and forth between these two planes — the shapes of ellipses are not preserved (except, of course, in the special case – which is precisely that of isotropy – when the ellipses degenerate to circles). Eigenvectors are determined by the directions in which the points of contact of these two curves lie (indicated by red circles).

Figures 1 and 2 present an example based on a glassy material. Typical values for the bulk and shear moduli of glass were used: $K_m = 46.3$ GPa and $G_m = 30.5$ GPa, respectively. The value of the Biot-Willis coefficient was arbitrarily chosen as $\alpha = 0.6$, so $K^d_R = 18.52$ GPa. Taking Poisson's ratio as $\nu_d = 0.2$, we have $G_d = 13.89$ GPa. Skempton's coefficient was chosen for simplicity to be $B \equiv 1$ in this and all the other examples as well. (This choice is extreme because it implies that $K^u_R = K_m$. But, since our interest here is in analysis of the undrained shear modulus, the study of this limit is particularly useful to us.) The most anisotropic choices of β_1 and β_3 were used that would not produce absurd (negative) values of the diagonal coefficients for either s^u_{ij} or c^u_{ij}, and that also would not produce $G^*_u > G_m$.

For glass, these values were found to be $\beta_1 = 0.15\alpha/K_R^d$ and $\beta_3 = 0.70\alpha/K_R^d$. The value of the energy used for normalization was $U = 900.0$ GPa. Computed values for the effective and undrained shear moduli were $G_u^v = 25.43$ GPa and $G_u^* = 15.28$ GPa.

The second example considered is Schuler-Cotton Valley sandstone. Values used for the moduli of samples are taken from results contained in Berryman (2004b), wherein certain laboratory data were fitted using an elastic differential effective medium scheme. These results are summarized in TABLE 1.

Figures 3 and 4 present results for Schuler-Cotton Valley sandstone. Laboratory data on this material were also presented by Murphy (1982). The values chosen for β_1 and β_3 were $\beta_1 = 0.20\alpha/K_R^d$ and $\beta_3 = 0.60\alpha/K_R^d$. The value of the energy per unit volume used for normalization was $U \simeq 900.0$ GPa. Computed values for the effective and undrained shear moduli were $G_u^v = 35.8$ GPa and $G_u^* = 17.7$ GPa.

Discussion of estimates

We can compare the results obtained here with results obtained for the same porous materials using differential effective medium theory to fit data. Two characteristics concern us: (a) comparisons between the values chosen in our examples for the anisotropic β's and the best fitting crack aspect ratios found in Berryman (2004b), and (b) comparisons between the magnitudes of changes in the overall shear moduli from their drained to undrained values.

The preferred crack aspect ratio found for Schuler-Cotton Valley sandstone in Berryman (2004b) was 0.015. We found that (β_1', β_3') for Schuler-Cotton Valley sandstone was (0.20,0.60). Observed increase in shear modulus of the measured laboratory data for Schuler-Cotton Valley sandstone was about 10%. As seen in TABLE 1, the magnitude of the change predicted here is also about 10%. We also know from related work in Berryman (2004c) that the maximum undrained effect on shear for any heterogeneous porous medium is a 20% increase. So values observed here (and in other work) of about 10% can be considered typical. Thus, agreement is good both qualitatively and semi-quantitatively in all cases. The theory presented correctly estimates the observed magnitudes of these shear modulus enhancements due to pore-fluid effects.

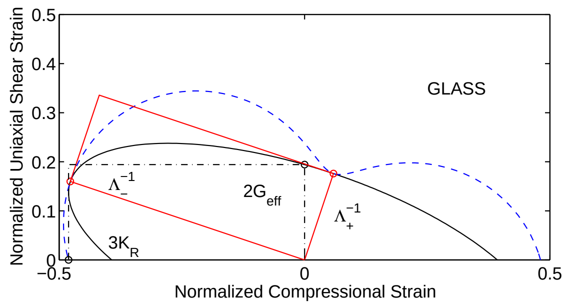

FIG. 1: For a glassy porous material having bulk modulus $K_{dr} = 18.52$ GPa and shear modulus $G_{dr} = 13.89$ GPa, the locus of points $z = Re^{i\theta}$ [see equation (44)] having constant energy $U = 900$ GPa, when the linear combination of pure compression and pure uniaxial shear is interpreted as strain field applied to the stiffness matrix (solid black line). The plot is in the complex z-plane, with the inverse of the corresponding expression for the compliance energy superposed for comparison (dashed blue line). Red circles at the two points of intersection correspond to the two eigenvalues/eigenvectors of the system of equations. The ellipse (solid black line) in this plane corresponds to the more complex curve in Figure 2. The two rectangles illustrate the product formula (19) derived and used in the text. The shapes of these rectangles are very similar, but not identical; however, their areas are identical.

BOUNDS AND SELF-CONSISTENT ESTIMATES

Rigorous methods such as the Hashin-Shtrikman bounds (Hashin and Shitrikman, 1962) exist for constraining the behavior of an overall isotropic composite medium whose constituents are anisotropic grains. For the types of crystal symmetry considered here (hexagonal, tetragonal, and cubic), Peselnick and Meister (1965), Meister and Peselnick (1966), and Watt and Peselnick (1980) have developed nontrivial expressions required to implement these bounds. Also, it has been shown recently by Berryman (2005b) that these methods can also be used to determine self-consistent estimates for these same types of composite media. For our present application, the main complication comes from the presence of pore-fluids and the fact that there are two calculations that are pertinent: one for drained and one for undrained pore fluid. As we have seen already in this paper, these types of complications are not difficult to incorporate into the analysis, since they just provide shifts from the drained compliances to the undrained compliances, as the pore-liquid tends to stiffen the porous medium in both compression and shear, when compared to the case with gas-filled pores.

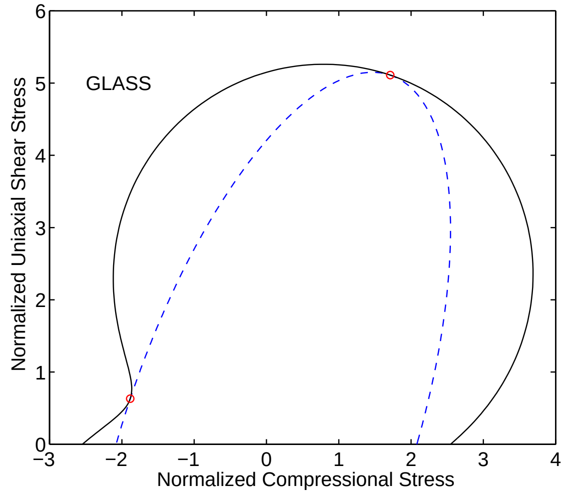

FIG. 2: Same parameters as Figure 1, but the linear combination of pure compression and pure uniaxial shear is interpreted as a stress field and is applied to the compliance matrix (dashed blue line). The plot is again in the complex z-plane, with the inverse of the corresponding expression for the stiffness energy superposed for comparison (solid black line). Red circles at the two points of intersection correspond to the two eigenvalues/eigenvectors of the system of equations. The ellipse (dashed blue line here) corresponds to the more complex curve in Figure 1.

Bounds on the bulk and shear moduli

Formulas for bounds on the bulk and shear moduli of random polycrystals having grains with hexagonal, trigonal, or tetragonal symmetries are the main results of Watt and Peselnick (1980) [based on the earlier work of Peselnick and Meister (1965) and Meister and Peselnick (1966)]. The author has shown recently that the analytical forms of these results can be considerably simplified. Derivations have been given elsewhere (Berryman, 2005b) and this analysis will not be repeated here. The bulk modulus results for all these symmetries are given in the same format by

$$K_{PM}^{\pm} = \frac{K_V(G^r + \zeta_\pm)}{(G^v + \zeta_\pm)}, \tag{45}$$

where the formula applies to either drained or undrained cases with appropriate factors used on the right hand side of the equation. The shear moduli G^r and G^v have the same significance here as they did in (19), (22), (23), (24), etc. The parameters $\zeta_\pm$ are defined by

$$\zeta_\pm = \frac{G_\pm}{6}\left(\frac{9K_\pm + 8G_\pm}{K_\pm + 2G_\pm}\right). \tag{46}$$

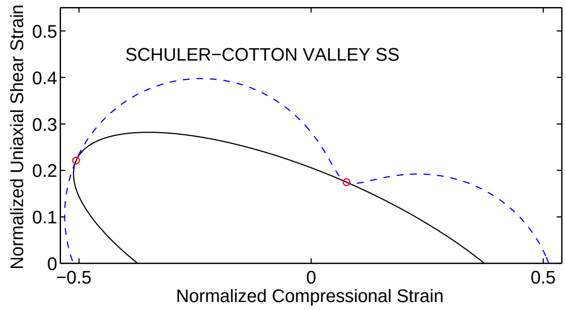

FIG. 3: For Schuler-Cotton Valley Sandstone (Murphy, 1982) having bulk modulus $K_{dr} = 13.1$ GPa and shear modulus $G_{dr} = 15.7$ GPa, the locus of points $z = Re^{i\theta}$ [see equation (34***)] having constant energy $U = 900$ GPa, when the linear combination of pure compression and pure uniaxial shear is interpreted as strain field applied to the stiffness matrix (solid black line). The plot is in the complex z-plane, with the inverse of the corresponding expression for the compliance energy superposed for comparison (dashed blue line). Red circles at the two points of intersection correspond to the two eigenvectors of the system of equations. The ellipse (solid black line) in this plane corresponds to the more complex curve in Figure 2.

In (46), the values of $G_\pm$ and $K_\pm$ are those defined algorithmically by

$$K_\pm = \frac{K_V(G^r - G_\pm)}{(G^v - G_\pm)}, \tag{47}$$

where, for K_-,

$$0 \le G_- \le \min(c_{44}, \mu_3, G^r, c_{66}) \qquad \text{(tetragonal)}, \tag{48}$$

recalling that $\mu_3 \equiv (c_{11} - c_{12})/2$. Similarly, for the K_+ formula,

$$\max(c_{44}, \mu_3, G^v, c_{66}) \le G_+ \le \infty \qquad \text{(tetragonal)}. \tag{49}$$

The results for shear modulus values of the various symmetry types differ somewhat, but — to illustrate these results — we will quote only the case of tetragonal symmetry, which is

$$\frac{1}{G^\pm_{\rm tetr} + \zeta_\pm} = \frac{1}{5}\left[\frac{1 - \pi_\pm(K_V - K_\pm)}{G^v + \zeta_\pm + \delta_\pm(K_V - K_\pm)} + \frac{1}{\mu_3 + \zeta_\pm} + \frac{2}{c_{44} + \zeta_\pm} + \frac{1}{c_{66} + \zeta_\pm}\right]. \tag{50}$$

The factor $\zeta_\pm$ is given as before by (46). And, the factors $\pi_\pm$ and $\delta_\pm$ are determined by

$$\pi_\pm = \frac{-1}{K_\pm + 4G_\pm/3}, \qquad \text{and} \qquad \delta_\pm = \frac{5G_\pm/2}{K_\pm + 2G_\pm}. \tag{51}$$

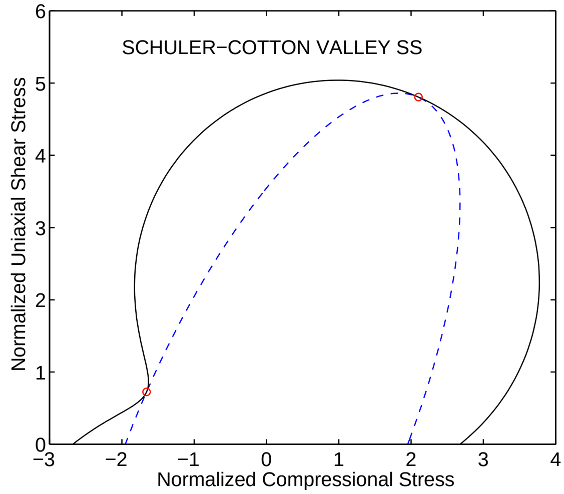

FIG. 4: Same parameters as Figure 1, but the linear combination of pure compression and pure uniaxial shear is interpreted as a stress field and is applied to the compliance matrix (dashed blue line). The plot is again in the complex z-plane, with the inverse of the corresponding expression for the stiffness energy superposed for comparison (solid black line). Red circles at the two points of intersection correspond to the two eigenvectors of the system of equations. The ellipse (dashed blue line here) corresponds to the more complex curve in Figure 1.

Self-consistent estimates of bulk and shear moduli

The self-consistent estimates for bulk modulus can be obtained by the straightforward operational method of simply replacing the parameters $K_\pm$, $G_\pm$, and $\zeta_\pm$ by the (to be determined) self-consistent values K^*, G^*, and ζ^*, respectively. So the resulting formula is

$$K^* = \frac{K_V(G^r + \zeta^*)}{(G^v + \zeta^*)} = \frac{(G^v K_R + \zeta^* K_V)}{(G^v + \zeta^*)}, \tag{52}$$

where

$$\zeta^* = \frac{G^*}{6}\left(\frac{9K^* + 8G^*}{K^* + 2G^*}\right). \tag{53}$$

For porous media, K_V, G^r, G^v, and K_R are all evaluated either for drained or for undrained values depending on the application.

To arrive at the correct formulation of the self-consistent shear modulus, we must be careful to apply a correction related to the fact that the bounds are actually defined along a specific trajectory (47) in the $(G_\pm, K_\pm)$-plane. When we are not on this curve, there is a factor in the denominator of the first term on the right hand side that cancels the term proportional to δ in (50). The final result for tetragonal symmetry is then given by:

$$\frac{1}{G^*_{\text{tetr}}+\zeta^*}=\frac{1}{5}\left[\frac{1-\pi^*(K_V-K^*)}{G^v_{\text{eff}}+\zeta^*}+\frac{1}{\mu_3+\zeta^*}+\frac{2}{c_{44}+\zeta^*}+\frac{1}{c_{66}+\zeta^*}\right]. \tag{54}$$

The factor π^* is

$$\pi^*=\frac{-1}{K^*+4G^*/3}. \tag{55}$$

Very similar forms are also available for self-consistent shear modulus in the hexagonal, trigonal, and cubic cases. But, we will not discuss these results here.

TABLE 2. Elastic stiffness constants of tetragonal indium, mercurous chloride (Hg_2Cl_2), and urea ($CO(NH_2)_2$).

	In	Hg_2Cl_2	$CO(NH_2)_2$
c_{11} (GPa)	45.2	18.93	21.7
c_{12} (GPa)	40.0	17.19	8.9
c_{13} (GPa)	41.2	15.63	24.0
c_{33} (GPa)	44.9	80.37	53.2
c_{44} (GPa)	6.52	8.46	6.3
c_{66} (GPa)	12.00	12.25	0.45
μ_3 (GPa)	2.60	0.87	6.40
G^v (GPa)	1.70	22.39	6.83

Examples of bounds and various estimates

We can use the formulas (45) and (50) to bound the bulk and shear moduli of pure random polycrystals (having no porosity). The corresponding self-consistent estimates (52) and (54) can then be taken as reasonable estimators (K^*_m and μ^*_m) of the isotropic values of the constants for the pure polycrystal. We can then continue this process and produce bounds and estimates for the porous random polycrystal, in this case using well-known formulas for both bounds and estimates. If ϕ is porosity (volume fraction of void space), then the self-consistent drained constants are

$$\frac{1}{K^d_{SC}+4G^d_{SC}/3}=\frac{1-\phi}{K^*_m+4G^d_{SC}/3}+\frac{\phi}{4G^d_{SC}/3} \tag{56}$$

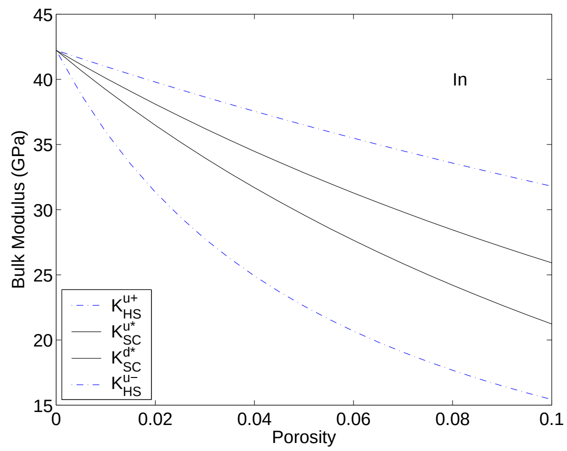

FIG. 5: Undrained bulk modulus bounds and self-consistent estimates for the porous indium, as a function of porosity. Input stiffnesses are listed in Table 2.

and

$$\frac{1}{G^d_{SC} + \zeta^d_{SC}} = \frac{1-\phi}{G^*_m + \zeta^d_{SC}} + \frac{\phi}{\zeta^d_{SC}}, \tag{57}$$

while the self-consistent undrained constants are

$$\frac{1}{K^u_{SC} + 4G^u_{SC}/3} = \frac{1-\phi}{K^*_m + 4G^u_{SC}/3} + \frac{\phi}{K_f + 4G^u_{SC}/3} \tag{58}$$

and

$$\frac{1}{G^u_{SC} + \zeta^u_{SC}} = \frac{1-\phi}{G^*_m + \zeta^u_{SC}} + \frac{\phi}{\zeta^u_{SC}}. \tag{59}$$

In both cases, $\zeta_{SC} = (G_{SC}/6)(9K_{SC} + 8G_{SC})/(K_{SC} + 2G_{SC})$.

Hashin-Shtrikman lower bounds for drained constants for both bulk and shear modulus are exactly zero for any finite value of porosity, which is also why the self-consistent estimates are of such importance for porous media. Hashin-Shtrikman upper bounds for drained constants are:

$$\frac{1}{K^{d+}_{HS} + 4G_+/3} = \frac{1-\phi}{K^*_m + 4G_+/3} + \frac{\phi}{4G_+/3} \tag{60}$$

and

$$\frac{1}{G^{d+}_{HS} + \zeta_+} = \frac{1-\phi}{G^*_m + \zeta_+} + \frac{\phi}{\zeta_+}, \tag{61}$$

where $G_+ = \max(c_{44}, \mu_3, G^v, c_{66})$ is the largest shear modulus in the system, and ζ_+ is computed using G_+ and $\max(K_f, K^*_m)$, which will usually be equal to K^*_m.

Hashin-Shtrikman upper and lower bounds for undrained constants are:

$$\frac{1}{K^{u\pm}_{HS} + 4G_\pm/3} = \frac{1-\phi}{K^*_m + 4G_\pm/3} + \frac{\phi}{K_f + 4G_\pm/3} \tag{62}$$

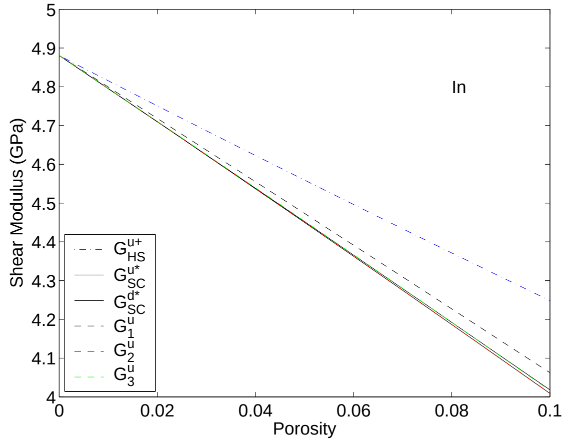

FIG. 6: Undrained shear modulus bounds, self-consistent estimates, and three examples of the analytical estimate from Equation (43) for the porous indium, as a function of porosity.

and

$$\frac{1}{G^{u\pm}_{HS} + \zeta_\pm} = \frac{1-\phi}{G^*_m + \zeta_\pm} + \frac{\phi}{\zeta_\pm}, \tag{63}$$

where $G_+ = \max(c_{44}, \mu_3, G^v, c_{66})$ and $G_- = 0$ are, respectively, the largest and smallest shear moduli in the system. The parameter ζ_+ is computed using G_+ and $\max(K_f, K^*_m)$, while $\zeta_- = 0$ always holds. It follows then that the Hashin-Shtrikman lower bound on undrained shear modulus also vanishes identically for any finite porosity, but the lower bound on undrained bulk modulus does not necessarily vanish as long as $K_f \neq 0$.

Finally, we also have analytical estimates to consider from (43). First note that we can express Skempton's coefficient B in terms of other quantities that will be computed (or measured), so that along with $\alpha = 1 - K_d/K_m$, we also have

$$B = \frac{1 - K_d/K_u}{\alpha}. \tag{64}$$

Therefore, the examples that follow are not restricted to the extreme case $B = 1$. Now, to simplify the expression in (43) somewhat, it is useful to note that

$$1 + K^d_R \tau_d = \frac{c_{33} - c_{13}}{2G^v_d}. \tag{65}$$

This expression is particularly relevant when $\beta'_3 = 1$ and $\beta'_1 = 0$ (recalling that $2\beta'_1 + \beta'_3 = 1$). Note that $K^d_R\tau_d + \beta'_3 - \beta'_1 = (1 + K^d_R\tau_d) - (1 + \beta'_1 - \beta'_3)$. Then, three cases are of most interest: (a) $\beta'_3 = 1$ (maximal effect of the fluid along the axis of grain symmetry), (b) $\beta'_1 = \beta'_3 = 1/3$ (soft isotropy), and (c) $\beta'_1 = 1/2$ (maximal effect of the fluid off the grain symmetry axis).

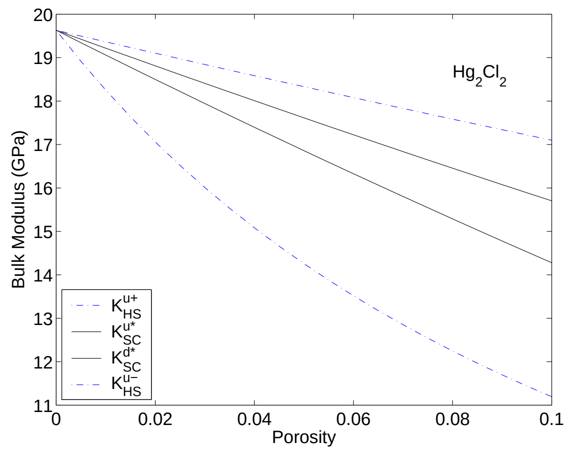

FIG. 7: Undrained bulk modulus bounds and self-consistent estimates for porous mercurous chloride (Hg_2Cl_2), as a function of porosity. Input stiffnesses are listed in TABLE 2.

Examples are presented for random polycrystals of porous indium, mercurous chloride (Hg_2Cl_2), and urea ($CO(NH_2)_2$). TABLE 2 presents the input elastic constants. Figures 5-10 display the results. For each case a pair of figures shows the results first for bulk modulus and then for shear modulus. Four curves for bulk modulus include two rigorous bounds — both for the undrained constants, and also two self-consistent curves — one for the drained constant and the other for the undrained constant. In each case the drained bulk modulus estimate lies below the undrained bulk modulus estimate and also below the undrained upper bound, as would be expected. perhaps surprisingly the drained estimate is however above the lower bound on the undrained bulk modulus in all three figures. The reason for this is that the lower bound for the undrained case is computed using the lowest shear modulus in the fluid-saturated system (which is zero), whereas the self-consistent estimate uses the self-consistent estimate of the shear modulus, which is always substantially above zero as is seen in the Figures for shear modulus. So there is no contradiction here, but there is some incompatibility between the assumptions of the various calculations and so care should be used when interpreting the results.

The most important results are those for the shear moduli shown in Figures 6, 8, and 10. The lower bounds for both drained and undrained shear modulus are zero at finite porosity, and so are not plotted. The Hashin-Shtrikman upper bound is always an upper bound on the self-consistent estimates, both undrained and drained. The drained estimates are always lower than the undrained as expected— although, in all three of these examples,

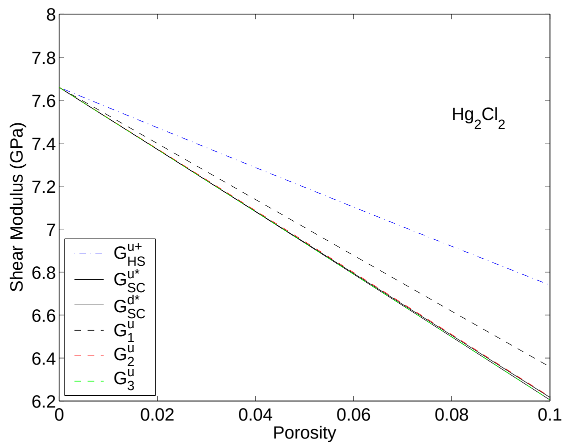

FIG. 8: Undrained shear modulus bounds, self-consistent estimates, and three examples of the analytical estimate from Equation (43) for porous mercurous chloride (Hg_2Cl_2), as a function of porosity.

the differences are not great.

The remaining estimates are the three special cases obtained from (43). G_1^u corresponds to $\beta_3' = 1$ (maximal axial effect of the fluid). G_2^u corresponds to $\beta_1' = \beta_3' = 1/3$, which is soft isotropy. And G_3^u corresponds to $\beta_1' = 1/2$ (minimal axial effect of the fluid). It is clear that G_1^u should always be give the largest estimate of these three, and this is observed in all three examples. The relationship between the remaining to cases is not so simple, as it depends not only on the values of the β's, but also on the hard anisotropy. If there is no hard anisotropy (or very little), then G_2^u will correspond to a completely (or almost totally) isotropic porous material, and so Gassmann's results will hold. In this very special case, G_2^u should take the same value as G_{SC}^*, assuming that the self-consistent calculation is compatible with the other estimate. We see in Figure 6 for indium this is essentially what happens. Then, the value of G_3^u must be higher than G_2^u, but not as high as G_1^u. This behavior is also observed in Figure 6. The results show in particular that the two types of estimators (G_{SC}^* and the G_i^u's for $i = 1, 2, 3$) are remarkably consistent, even though they have been obtained using very different arguments. In contrast, mercurous chloride shows a different behavior in Figure 8, having $G_2^u > G_3^u$. This means that the hard and soft anisotropy are effectively canceling each other in the overall result for this case.

Finally, urea is the most compliant of the crystals considered and, therefore, shows the greatest effect of the stiffening due to the pore fluid in Figure 10. Here we find again (as

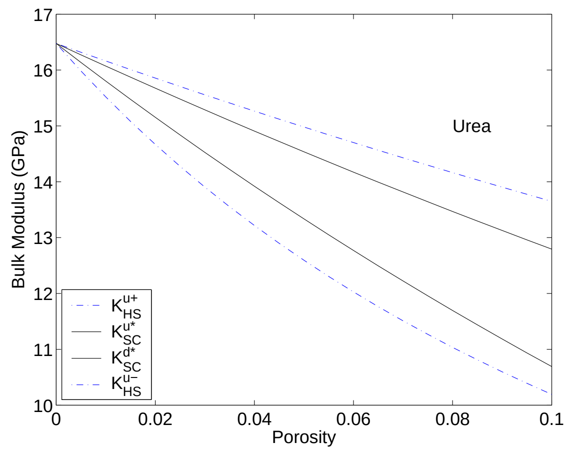

FIG. 9: Undrained bulk modulus bounds and self-consistent estimates for porous urea ($CO(NH_2)_2$), as a function of porosity. Input stiffnesses are listed in TABLE 2.

in Figure 8) that $G_1^u > G_2^u > G_3^u$. But, in this case, the stiffening effect is so strong for maximal axial effect of the fluid that $G_1^u > G_{HS}^{u+}$. The author has no immediate explanation for this effect. But it should be pointed out that in polycrystalline materials, it is possible for some special microgeometries that the overall stiffness can approach the Voigt average, and therefore exceed the Hashin-Shtrikman bound (Milton, 2002). It is not obvious that this is the correct explanation for the result observed, but it is one possible source of this apparent discrepancy.

SUMMARY AND CONCLUSIONS

Several different approaches to understanding pore-fluid enhanced shear modulus have been considered. The first result obtained was the physically motivated estimator in (43). This result has several advantages, including the ability to treat hard anisotropy and/or soft anisotropy either separately or simultaneously. The second type of estimator introduced was the self-consistent estimator (54), closely related to the rigorous (Hashin-Shtrikman-type) bounds for nonporous random polycrystals. These estimators were then used as input to another type of self-consistent estimator in order to generate both drained and undrained constants (57) and (59) for porous polycrystals. Finally, estimators and bounds were computed for three tetragonal polycrystals in order to compare and contrast these methods. We found excellent agreement between the first estimates from (43) and the self-consistent estimates (57) and (59). This agreement tends to cross-validate both methods used, since

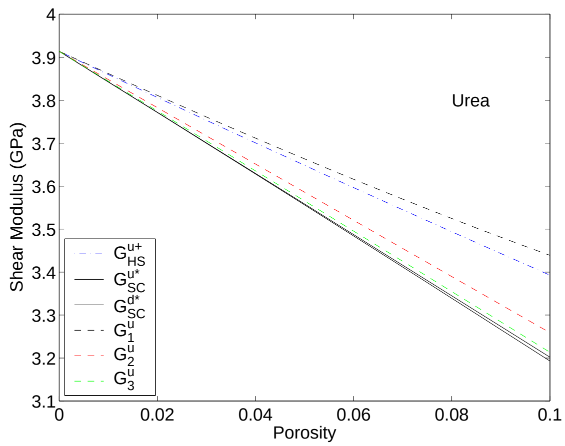

FIG. 10: Undrained shear modulus bounds, self-consistent estimates, and three examples of the analytical estimate from Equation (43) for porous urea ($CO(NH_2)_2$), as a function of porosity.

they are based on conceptually independent theoretical perspectives.

In porous media, under many circumstances, overall shear modulus depends on pore-liquid mechanics. This dependence arises in any of the anisotropic media having the crystal symmetries considered (hexagonal, tetragonal, cubic), and others as well. The results demonstrate how compression-to-shear coupling enters the analysis for some anisotropic materials, and also how this coupling leads to the observed overall shear dependence on liquids trapped in pores.

These effects need not always be large. However, the effects can be fairly substantial — on the order of a 10% to 20% increase in the overall shear modulus — in cracked or fractured materials, when these pores are liquid-filled. Anisotropy and liquid stiffening effects both come strongly into play, as illustrated in Figures 1–4. In particular, if $\beta_1 \simeq \beta_3$, then soft anisotropy does not make a significant contribution. But, if either $\beta_1 << \beta_3$ or $\beta_1 >> \beta_3$, then the contribution can be significant. Analytical results summarized in (43) have also been compared to bounds and self-consistent effective medium results in Figures 5-10.

ACKNOWLEDGMENTS

Work performed under the auspices of the U.S. Department of Energy under contract No. W-7405-ENG-48 and supported specifically by the Geosciences Research Program of the DOE Office of Basic Energy Sciences, Division of Chemical Sciences, Geosciences and Biosciences. Work also supported in part by the Stanford Exploration Project, while on sabbatical visiting the Geophysics Department at Stanford University.

APPENDIX A

The equation of an ellipse centered at the origin whose semi-major and semi-minor axes are of lengths a and b and whose angle of rotation with respect to the x-axis in the (x, y)-plane is ψ is given by

$$(x \cos\psi + y \sin\psi)^2/a^2 + (-x \sin\psi + y \cos\psi)^2/b^2 = 1. \tag{66}$$

For comparison, when a stress of magnitude $r = \sqrt{x^2 + y^2}$ is applied to a poroelastic system, the energy stored in the anisotropic media of interest here [using (16) and (25)] is given by

$$\begin{aligned} U(r,\theta) &= 3r^2 \left[A_{11} \cos^2\theta + 2\sqrt{2} A_{13} \cos\theta \sin\theta + 2A_{33} \sin^2\theta \right] \\ &= R^2 U(r_0, \theta), \end{aligned} \tag{67}$$

where in the second equation $R \equiv r/r_0$, and r_0 in an arbitrary number (say unity) having the dimensions of stress (*i.e.*, dimensions of Pa). It is not hard to see that, when $U(r,\theta) = const$, the two equations (66) and (67) have the same functional form and, therefore, that contours of constant energy in the complex $(z = x + iy)$ plane are ellipses. Furthermore, we can solve for the parameters of the ellipse by setting $U = 1$ (in arbitrary units for now) in (67) and then factoring r^2 out of both equations. We find that

$$\begin{aligned} 3A_{11} &= \frac{\cos^2\psi}{a^2} + \frac{\sin^2\psi}{b^2}, \\ 6\sqrt{2}A_{13} &= \sin 2\psi \left(\frac{1}{a^2} - \frac{1}{b^2} \right), \\ 6A_{33} &= \frac{\sin^2\psi}{a^2} + \frac{\cos^2\psi}{b^2}. \end{aligned} \tag{68}$$

These three equations can be inverted for the parameters of the ellipse, giving:

$$\begin{aligned} \frac{1}{a^2} &= \frac{3A_{11}\cos^2\psi - 6A_{33}\sin^2\psi}{\cos 2\psi}, \\ \frac{1}{b^2} &= -\frac{3A_{11}\sin^2\psi - 6A_{33}\cos^2\psi}{\cos 2\psi}, \\ \tan 2\psi &= \frac{2\sqrt{2}A_{13}}{A_{11} - 2A_{33}}. \end{aligned} \tag{69}$$

Although contours of constant energy are of some interest, it is probably more useful to our intuition for the poroelastic application to think instead about contours associated with applied stresses and strains of unit magnitude, *i.e.*, for $r = 1$ (in appropriate units) and θ

varying from 0 to π. We then have the important function $U(1,\theta)$. [Note that, when θ varies instead between π and 2π, we just get a copy of the behavior for θ between 0 and π. The only difference is that the stress and strain vectors have an overall minus sign relative to those on the other half-circle. For a linear system, such an overall phase factor of unit magnitude is irrelevant to the mechanics of the problem.] Then, if we set $U(r,\theta) = const = R^2U(r_0,\theta)$ and plot $z = Re^{i\theta}$ in the complex plane, we will have a plot of the ellipse of interest with R determined analytically by

$$R = \sqrt{U(r,\theta)/U(r_0,\theta)} = \sqrt{const/U(r_0,\theta)}. \tag{70}$$

We call R the magnitude of the normalized stress (*i.e.*, normalized with respect to r_0).

The analysis just outlined can then be repeated for the stiffness matrix and applied strain vectors. The mathematics is completely analogous to the case already discussed, so we will not repeat it here. Since strain is already a dimensionless quantity, the factor that plays the same role as r_0 above can in this case be chosen to be unity if desired, as the main purpose of the factor r_0 above was to keep track of the dimensions of the stress components.

APPENDIX B: PROOF OF PRODUCT FORMULAS

The product formula (39) was first presented in Berryman (2004a), where two derivations of this formula were also given. A different derivation is provided here, based on singular value decomposition of the pertinent reduced (2×2) matrix.

Using the definitions of unit trial vector f and reduced (*i.e.*, 2×2) compliance matrix Σ^* from Eqs. (25) and (16), we can immediately write the eigenvalue (or singular value) decomposition of the matrix Σ^* in terms of its eigenvectors and eigenvalues $f(\theta_\pm)$ and $\Lambda_\pm$. The result is

$$\Sigma^* = f(\theta_+)\Lambda_+ f^T(\theta_+) + f(\theta_-)\Lambda_- f^T(\theta_-). \tag{71}$$

The reduced stiffness matrix is just the inverse of Σ^*, and so is represented similarly by

$$(\Sigma^*)^{-1} = f(\theta_+)\Lambda_+^{-1} f^T(\theta_+) + f(\theta_-)\Lambda_-^{-1} f^T(\theta_-). \tag{72}$$

The curves in Figures 1–4 can then all be parametrized in terms of polar angle θ by considering the formulas

$$f^T(\theta)\Sigma^* f(\theta) = \Lambda_+ \cos^2(\theta - \theta_+) + \Lambda_- \cos^2(\theta - \theta_-) \tag{73}$$

for compliance, and

$$f^T(\theta)\,(\Sigma^*)^{-1}\,f(\theta) = (\Lambda_+)^{-1}\cos^2(\theta-\theta_+) + (\Lambda_-)^{-1}\cos^2(\theta-\theta_-) \tag{74}$$

for stiffness.

Then, the undrained bulk modulus of the system $K_u = K_R$ is found from (71) to be

$$(3K_R)^{-1} = \overline{v}_1^T\Sigma^*\overline{v}_1 = \Lambda_+\cos^2\theta_+ + \Lambda_-\cos^2\theta_-. \tag{75}$$

Similarly, the effective undrained shear modulus G_{eff} by definition is determined from

$$2G_{eff} = \overline{v}_3^T\,(\Sigma^*)^{-1}\,\overline{v}_3 = \Lambda_+^{-1}\sin^2\theta_+ + \Lambda_-^{-1}\sin^2\theta_-. \tag{76}$$

Taking the ratio of these quantities of interest, we find easily that

$$\frac{1}{6K_RG_{eff}} = \frac{\Lambda_+\cos^2\theta_+ + \Lambda_-\cos^2\theta_-}{\Lambda_+^{-1}\sin^2\theta_+ + \Lambda_-^{-1}\sin^2\theta_-} = \Lambda_+\Lambda_-, \tag{77}$$

where the final equality follows directly from the identity

$$\sin^2\theta_- = \sin^2\left(\theta_+ + \frac{\pi}{2}\right) = \cos^2\theta_+. \tag{78}$$

Eq. (77) is a special case of a more general product formula, true for any angle θ, which follows from the identity

$$\begin{aligned} f^T(\theta)\Sigma^*f(\theta)/\sqrt{\Lambda_+\Lambda_-} &= \sqrt{\frac{\Lambda_+}{\Lambda_-}}\cos^2(\theta-\theta_+) + \sqrt{\frac{\Lambda_-}{\Lambda_+}}\cos^2(\theta-\theta_-) \\ &= f^T(\theta+\pi/2)\,(\Sigma^*)^{-1}\,f(\theta+\pi/2)/\sqrt{\Lambda_+^{-1}\Lambda_-^{-1}} \end{aligned} \tag{79}$$

and is straighforward to verify.

Equation (77) is the product formula quoted in equation (39), and first derived in Berryman (2004a). A geometrical interpretation of the formula is obtained by considering, for example, Figure 1. A plane rectangle is formed by considering the origin and the two points labeled by $(\Lambda_+)^{-1}$ and $(\Lambda_-)^{-1}$ to be three of the four vertices of this rectangle. The area of this rectangle is clearly the product $(\Lambda_+\Lambda_-)^{-1}$. Similarly, the plane rectangle formed in the same way from the origin and the points labeled $2G_u^v$ and $3K_R^u$ clearly has area $6G_u^vK_R^u$. It is seen in Figure 1 that, at least to graphical accuracy, these two rectangles are practically indistinguishable — although in fact they are not identical in shape. Formula (77) shows further that the areas of these two rectangles are always equal.

REFERENCES

Backus, G. E. (1962). Long-wave elastic anisotropy produced by horizontal layering, *J. Geophys. Res.*, **67**: 4427–4440.

Berge, P. A., and Berryman, J. G. (1995). Realizability of negative pore compressibility in poroelastic composites, *ASME J. Appl. Mech.*, **62**: 1053–1062.

Berryman, J. G. (1999). Origin of Gassmann's equations, *Geophysics*, **64**: 1627–1629.

Berryman, J. G. (2004a). Poroelastic shear modulus dependence on pore-fluid properties arising in a model of thin isotropic layers, *Geophys. J. Int.*, **157**: 415–425.

Berryman, J. G. (2004b). Modeling high-frequency acoustic velocities in patchy and partially saturated porous rock using differential effective medium theory, *Int. J. Multiscale Computational Engineering*, **2**: 115–131.

Berryman, J. G. (2004c). Bounds on elastic constants for random polycrystals of laminates, *J. Appl. Phys.* **96**, 4281–4287.

Berryman, J. G. (2005a). Fluid effects on shear waves in finely layered porous media, *Geophysics*, in press.

Berryman, J. G. (2005b). Bounds and estimates for elastic constants of random polycrystals of laminates, *Int. J. Solids Structures*, in press.

Berryman, J. G., and Milton, G. W. (1991). Exact results for generalized Gassmann's equations in composite porous media with two constituents, *Geophysics*, **56**: 1950–1960.

Berryman, J. G., and Thigpen, L. (1985). Nonlinear and semilinear dynamic poroelasticity with microstructure, *J. Mech. Phys. Solids*, **33**: 97–116.

Berryman, J. G., and Wang, H. F. (1995). The elastic coefficients of double-porosity models for fluid transport in jointed rock, *J. Geophys. Res.*, **100**: 24611–24627.

Berryman, J. G., and Wang, H. F. (2001). Dispersion in poroelastic systems, *Phys. Rev. E*, **64**: paper: 011303.

Berryman, J. G., Berge, P. A., and Bonner, B. P. (2002a). Estimating rock porosity and fluid saturation using only seismic velocities, *Geophysics*, **67**: 391–404.

Berryman, J. G., Pride, S. R., and Wang. H. F. (2002b). A differential scheme for elastic properties of rocks with dry or saturated cracks, *Geophys. J. Int.*, **151**: 597–611.

Biot, M. A. (1962). Mechanics of deformation and acoustic propagation in porous media, *J. Appl. Phys.*, **33**: 1482–1498.

Biot, M. A., and Willis, D. G. (1957). The elastic coefficients of the theory of consolidation, *J. Appl. Mech.*, **24**: 594–601.

Brown, R. J. S., and Korringa, J. (1975). On the dependence of the elastic properties of a porous rock on the compressibility of a pore fluid, *Geophysics*, **40**: 608–616.

Gassmann, F. (1951). Über die elastizität poröser medien, *Veirteljahrsschrift der Naturforschenden Gesellschaft in Zürich*, **96**: 1–23.

Hashin, Z., and Shtrikman, S. (1962). A variational approach to the theory of the elastic behaviour of polycrystals, *J. Mech. Phys. Solids*, **10**: 343–352.

Hudson, J. A. (1981). Wave speeds and attenuation of elastic waves in material containing cracks, *Geophys. J. R. Astr. Soc.*, **64**: 133–150.

Knight, R., and Nolen-Hoeksema, R. (1990). A laboratory study of the dependence of elastic wave velocities on pore scale fluid distribution, *Geophys. Res. Lett.*, **17**: 1529–1532.

Mavko, G., and Jizba, D. (1991). Estimating grain-scale fluid effects on velocity dispersion in rocks, *Geophysics*, **56**: 1940–1949.

Meister, R., and Peselnick, L. (1966). Variational method of determining effective moduli of polycrystals with tetragonal symmetry, *J. Appl. Phys.*, **37**, 4121–4125.

Milton, G. W. (2002). *The Theory of Composites*, Cambridge University Press, Cambridge, UK, pp. 487–490.

Mukerji, T., and Mavko, G. (1994). Pore fluid effects on seismic velocity in anisotropic rocks, *Geophysics*, **59**: 233–244.

Murphy, William F., III (1982). *Effects of Microstructure and Pore Fluids on the Acoustic Properties of Granular Sedimentary Materials*, Ph.D. Dissertation, Stanford University.

Nye, J. F. (1957). *Physical Properties of Crystals: Their Representation by Tensors and Matrices*, Oxford Science Publications, Oxford.

O'Connell, R. J., and Budiansky, B. (1974). Seismic velocities in dry and saturated cracked solids, *J. Geophys. Res.*, **79**: 5412–5426.

Peselnick, L., and Meister, R. (1965). Variational method of determining effective moduli of polycrystals: (A) Hexagonal symmetry, (B) trigonal symmetry, *J. Appl. Phys.*, **36**, 2879–2884.

Rice, J. R., and Cleary, M. P. (1976). Some basic stress diffusion solutions for fluid-saturated elastic porous media with compressible constituents, *Rev. Geophys.*, **14**: 227–241.

Skempton, A. W. (1954). The pore-pressure coefficients A and B, *Geotechnique*, **4**: 143–147.

Walsh, J. B. (1969). New analysis of attenuation in partially melted rock, *J. Geophys. Res.*, **74**: 4333–4337.

Watt, J. P., and Peselnick, L. (1980). Clarification of the Hashin-Shtrikman bounds on the effective elastic moduli of polycrystals with hexagonal, trigonal, and tetragonal symmetries, *J. Appl. Phys.*, **51**, 1525–1531.

This work was performed under the auspices of the U.S. Department of Energy by University of California, Lawrence Livermore National Laboratory under contract W-7405-Eng-48.